Dalton Transactions

ROYAL SOCIETY OF CHEMISTRY

PAPER

View Article Online
View Journal | View Issue

Open Access Article. Published on 15 August 2023. Downloaded on 2/10/2026 5:32:21 PM.
This article is licensed under a Creative Commons Attribution 3.0 Unported Licence.

Check for updates

Cite this: *Dalton Trans.*, 2023, **52**, 12885

Two new red-emitting ternary europium(III) complexes with high photoluminescence quantum yields and exceptional performance in OLED devices†

Rashid Ilmi, *[a] Xiaofang Li,[b] Nawal K. Al Rasbi,[a] Liang Zhou, *[b] Wai-Yeung Wong, *[c] Paul R. Raithby *[d] and Muhammad S. Khan *[a]

Received 7th July 2023,
Accepted 14th August 2023

DOI: 10.1039/d3dt02147e

rsc.li/dalton

Two new organo-europium complexes (OEuCs) [Eu(btfa)$_3$(Bathphen)] (**OEuC-1**) and [Eu(tta)$_3$(Bathphen)] (**OEuC-2**) where btfa and tta are the anions of 4,4,4-trifluoro-1-phenyl-1,3-butanedione and 2-thenoyltrifluoroacetone while Bathphen = Bathophenanthroline have been synthesized and characterized. Both complexes in the solid state exhibit strong red emissions with photoluminescence quantum yields (PLQYs) of 80% ± 10%. These complexes were tested as dopants in the emitting layer (EML) to fabricate red organic light emitting diodes (R-OLEDs). Through device engineering involving the amalgamation of appropriate host materials and complexes, we have achieved exceptional overall R-OLED performance for an **OEuC-2** based device, with maximum current efficiency (CE_{max}) = 9.91 cd A^{-1}, maximum power efficiency (PE_{max}) = 9.15 lm W^{-1}, maximum external quantum efficiency ($EQE_{max.}$) = 6.24%, brightness (*B*) of 545 cd m^{-2}, and $(CIE)_{x,y}$ = 0.620, 0.323 at *J* = 10 mA cm^{-2}.

1 Introduction

Luminescent organo-lanthanide complexes (OLnCs), especially trivalent OEuCs, have been extensively applied in luminescence thermometry,[1] sensors[2] and OLED devices,[3] because of their innate optical properties.[4] In pursuit of OLED efficiency, it is vital that the complexes exhibit excellent photoluminescence quantum yields (PLQYs) *i.e.* >50% along with good electron-transport properties. A wide variety of bidentate chelating ligands have been tailored to develop OEuCs for this purpose.[5] Among them, mono-ionic β-diketone bidentate ligands in combination with neutral N^N ligands dominate. A search of the literature indicates that the PLQY of eight-coordinate [Eu(β-diket.)$_3$(*N*^*N*)] with a EuO_6N_2 coordination sphere rarely achieves 70% target (Table S1 and Chart S1, ESI†). This is because Eu(III) luminescence in OEuCs can be quenched readily by high-energy X–H oscillators[6] present in the organic ligands. Two complexes that do show a greater than 70% PLQY are deuterated hexafluoroacetylacetone (hfaa) systems bearing derivatives of phosphine oxide (O^O) as neutral ancillary ligands, *i.e.*, [Eu(hfa-D)$_3$(TPPO)$_2$] (PLQY = 90%)[7] and [Eu(hfa-D)$_3$(BIPHEPO)] (PLQY = 87%)[7] (Table S2 and Chart S2, ESI†) with a EuO_6O_2 coordination sphere [TPPO = triphenylphosphine oxide and BIPHEPO = 1,1′-biphenyl-2,2′-diyl bis(diphenylphosphineoxide)]. However, despite the very high PLQY, the potential application of these two complexes as EMLs in OLEDs has not been explored. Moreover, as observed by Kalyakina *et al.*,[8] despite having record PLQYs, ternary europium complexes of carboxylates bearing neutral phenanthroline (Phen) resulted in inferior electroluminescence (EL), due to the poor electron mobility of the Phen ligand. Even though the role of neutral ancillary ligand(s) in sensitizing the PL is almost two times lower (~35–25%) than that of primary anionic antenna ligand(s) (~65–75%),[9] their presence improves the physicochemical properties of OEuCs such as thermal stability, volatility, *etc.*[10] More importantly, they enhance the optoelectronic performance by serving as the main channel for charge and exciton harvesting.

[a]*Department of Chemistry, Sultan Qaboos University, P. O. Box 36, Al Khod 123, Oman. E-mail: rashidilmi@gmail.com, msk@squ.edu.om*
[b]*State Key Laboratory of Rare Earth Resource Utilization, Changchun Institute of Applied Chemistry, Chinese Academy of Sciences, Renmin Street 5625, Changchun 130022, People's Republic of China. E-mail: wai-yeung.wong@polyu.edu.hk*
[c]*Department of Applied Biology and Chemical Technology, The Hong Kong Polytechnic University, Hung Hom, Kowloon, Hong Kong, People's Republic of China. E-mail: zhoul@ciac.ac.cn*
[d]*Department of Chemistry, University of Bath, Claverton Down, Bath, BA2 7AY, UK. E-mail: p.r.raithby@bath.ac.uk*

†Electronic supplementary information (ESI) available. CCDC 2264545. For ESI and crystallographic data in CIF or other electronic format see DOI: https://doi.org/10.1039/d3dt02147e

Open Access Article. Published on 15 August 2023. Downloaded on 2/10/2026 5:32:21 PM.
This article is licensed under a Creative Commons Attribution 3.0 Unported Licence.

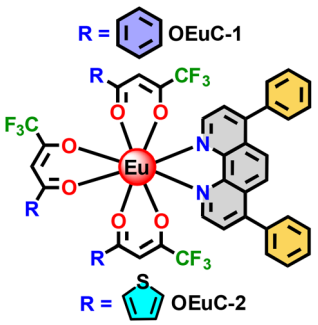

Chart 1 The molecular structure of the novel OEuCs.

In order to improve the EL performance of relatively cheap and easily accessible red-emitting OEuCs [crustal abundance 0.3 ppm][11] that can be compared to better known but expensive red-emitting iridium (Ir)-based complexes [crustal abundance 0.000037 ppm],[11] we embarked on the design and development of two new luminescent OEuCs (Chart 1) with a EuO_6N_2 coordination sphere. Compared to the preparation of many red-emitting Ir(III)-complexes which require specialized synthetic modifications and complicated purification processes,[12] Eu(III)-based complexes are relatively easy to prepare and exhibit highly efficient monochromatic red emissions (CIE ≈ 0.67, 0.33).[13] These Eu(III) complexes have a few basic prerequisites: strong light absorption properties of the ligand (s) and appropriate energy differences (ΔE)[14] between the $^3\pi\pi^*$ (triplet) and $^1\pi\pi^*$ (singlet) states. We now report the synthesis, characterization, and photophysical and electrophysical properties of two strongly luminescent OEuCs (Chart 1) with a EuO_6N_2 coordination sphere. This is achieved by employing readily available primary antenna ligands, Hbtfa and Htta ($^3\pi\pi^*$ = 21 400 cm^{-1} for btfa and 20 300 cm^{-1} for tta)[15] bearing an electron-donating phenyl/thienyl group at one terminus and an electron-withdrawing trifluoromethyl ($-CF_3$) group at the other terminus, which also play a pivotal role in minimising the vibrational quenching.[6] The rigid neutral Bathphen ligand with an extended π-system ($^3\pi\pi^*$ = 21 000 cm^{-1})[16] is employed as the ancillary ligand. It has good electron mobility (5×10^{-4} cm^2 V^{-1} s^{-1})[17] and has been widely used as a hole or exciton-blocking layer.

2 Experimental

2.1 Chemical reagents and general instrumentation

All chemicals used in the synthesis and OLED fabrication were purchased from commercial sources and were used without further purification unless otherwise specified. Solvents used in the experiments were dried and distilled prior to use. Elemental analyses of **OEuC-1** and **OEuC-2** were performed on a Euro EA-CHN elemental analyser. The Fourier transform infrared (FT-IR) spectra of the solid complexes were obtained using a Cary 630 FT-IR spectrometer in the attenuated total reflectance (ATR) mode. Mass spectra were obtained using an LCMS-8040, Shimadzu-Japan coupled to a triple quadruple tandem mass spectrometer equipped with electrospray ionization (ESI). The thermal stability of the complexes was determined by thermogravimetric analysis (TGA) and differential thermogravimetric analysis (DTA) in the temperature range between 50 and 700 °C under a dinitrogen (N_2) atmosphere and recorded on a TA Instruments model SDT Q600.

2.2 Synthesis

[Eu(btfa)$_3$(Bathphen)] (OEuC-1). **OEuC-1** was synthesized by reacting equimolar quantities of $[Eu(btfa)_3(H_2O)_2]$[13] (0.300 g, 0.360 mmol) and Bathphen (0.119 g, 0.360 mmol) in methanol (MeOH, 20 mL). The reaction mixture was stirred overnight at room temperature and left for slow solvent evaporation. The solid formed was washed with cold EtOH (5 × 2 mL) and toluene (5 × 2 mL). Yield: 80%. Microanalysis calculated for $C_{54}H_{34}EuF_9N_2O_6$, C, 57.41; H, 3.03; N, 2.48; observed C, 57.45; H, 3.01; N, 2.49%. FT-IR (solid, cm^{-1}): ν(ar C–H st) 3058 cm^{-1}; ν(C=O st) 1609 cm^{-1}; ν(C=N st) 1576 cm^{-1}; ν(C=C st) 1519 cm^{-1}; ν(C–F st, CF_3) 1388, 1317 cm^{-1}; out-of plane asymmetric ν(C–F st) 1180 cm^{-1}; in-plane ν(C–H bend) 1129 cm^{-1} (Fig. S1, ESI†); MS (positive mode): m/z: 1130.9 $[M + H]^+$; 1186.8 $[M + Na + CH_3OH + H]^+$ (Fig. S2, ESI†); decomposition temperature (T_d) with 5% weight loss = 315 °C (Fig. S3, ESI†).

[Eu(tta)$_3$(Bathphen)] (OEuC-2). **OEuC-2** was synthesized by a similar method with $[Eu(tta)_3(H_2O)_2]$[9b] (0.300 g, 0.305 mmol) and Bathphen (0.101 g, 0.305 mmol) in methanol (MeOH; 20 mL). Yield: 75%. Microanalysis calculated for $C_{48}H_{28}EuF_9N_2O_6S_3$, C, 50.23; H, 2.46; N, 2.44; observed C, 50.29; H, 2.41; N, 2.41%. FTIR (solid, cm^{-1}) ν(ar C–H st) 3096 cm^{-1}; ν(C=O st) 1625 cm^{-1}; ν(C=N st) 1594 cm^{-1}; ν(C=C st) 1507 cm^{-1}; ν(C–F st, CF_3) 1353, 1302 cm^{-1}; out-of plane asymmetric ν(C–F st) 1181 cm^{-1}; in-plane ν(C–H bend) 1127 cm^{-1} (Fig. S4, ESI†); MS (positive mode): m/z: 1200.9 $[M + Na + CH_3OH - H]^+$ (Fig. S5, ESI†); T_d with 5% weight loss = 330 °C (Fig. S6, ESI†).

2.3 Spectroscopic measurements, determination of photophysical parameters and the OLED fabrication process

Spectroscopic measurements of the complexes, which include UV-visible absorption, excitation, emission spectra, decay profiles and absolute PLQY values were obtained at room temperature; details of the measurements have been reported previously.[13] Optical absorption spectra were obtained using a Varian Cary 5000 UV-visible-NIR spectrophotometer while excitation, emission spectra and decay profiles were recorded on an Edinburgh FS5 fluorimeter. The absolute PLQYs of OEuCs in the solid state were determined using a Hamamatsu, C-9920-02 spectrometer equipped with a calibrated integrating sphere of 3.3 inches in radius and measured within the range of 300–750 nm. Excitation was provided with a 150 W xenon lamp after passing through a monochromator. The powder was pressed directly into the sample holder provided by the manufacturer. Photophysical parameters such as the *J–O* parameters (Ω_2 and Ω_4), A_{Rad}, A_{NRad} decay rates, radiative lifetime

 This journal is © The Royal Society of Chemistry 2023

Open Access Article. Published on 15 August 2023. Downloaded on 2/10/2026 5:32:21 PM.
This article is licensed under a Creative Commons Attribution 3.0 Unported Licence.

(τ_{rad}), Q_{Eu}^{Eu} and η_{sen} were calculated by applying the following set of equations and details are reported elsewhere.[18]

$$\Omega_{\lambda}^{exp} = \frac{3\hbar A_{Rad}[^5D_0 \rightarrow {}^7F_J]}{32e^2\pi^3\chi\nu[^5D_0 \rightarrow {}^7F_J]^3\left|\left\langle {}^5D_0\|U^{(\lambda)}\|{}^7F_J\right\rangle\right|^2} \quad (1)$$

$$A_{Rad} = \sum_{J=0}^{4} A_{Rad}[^5D_0 \rightarrow {}^7F_J] \quad (2)$$

$$A_{Rad}\left[^5D_0 \rightarrow {}^7F_J\right] = \frac{\nu[^5D_0 \rightarrow {}^7F_1]}{\nu[^5D_0 \rightarrow {}^7F_J]} \times \frac{A[^5D_0 \rightarrow {}^7F_J]}{A[^5D_0 \rightarrow {}^7F_1]} A_{Rad}[^5D_0 \rightarrow {}^7F_1] \quad (3)$$

$$A_{tot} = \frac{1}{\tau_{obs}} = A_{Rad} + A_{NRad} \quad (4)$$

$$\tau_R = \frac{1}{A_{Rad}} \quad (5)$$

$$Q_{Eu}^{Eu} = \frac{\tau_{obs}}{\tau_{Rad}} = \frac{A_{Rad}}{A_{Rad} + A_{NRad}} \quad (6)$$

$$\eta_{sen} = \frac{Q_{Eu}^{L}}{Q_{Eu}^{Eu}} \quad (7)$$

Details of the structure determination by single crystal X-ray diffraction, semi-empirical Sparkle/PM7 modelling, device fabrication and instrumentation involved are described in sections 1.1–1.3 of the ESI.†

3 Results and discussion

3.1 Synthesis, characterization and structure determination

The complexes **OEuC-1** and **OEuC-2** were synthesized by employing a two-step method[9b,13] reported earlier and were characterized by elemental analysis, FT-IR spectroscopy and mass spectrometry (Fig. S1–S6, ESI†), which supports the formulation of the complexes shown in Chart 1. The structure of **OEuC-1** (Fig. 1) was established using single-crystal X-ray diffraction while the structure of **OEuC-2** was elucidated using the computational Sparkle/PM7 method (Fig. S7, ESI†). The data obtained are listed in Tables S3–S7, ESI.† Both complexes have similar average Eu–O bond distances ≈2.38 Å, which are well comparable to those of reported analogues.[19] The symmetry of the octa-coordinate EuO_6N_2 geometry around the Eu(III) centre was determined using the SHAPE software package.[20] **OEuC-1** adopts a distorted square antiprismatic geometry (D_{4d}; with a deviation of 0.715 from the idealized square antiprism, Fig. 1 and Table S8†) while **OEuC-2** exhibits a distorted triangular dodecahedral geometry (D_{2d}; with a deviation of 1.687 from the idealized triangular dodecahedron, Fig. S7b and Table S8, ESI†).

3.2 Photophysical studies

Optical absorption spectroscopy was employed to gain information on the light absorbing capability of the complexes. The electronic absorption spectra are similar (Fig. S8, ESI†) except for the change in the molar absorptivity value. The complexes displayed broad spectra in the region between 250 and 400 nm with λ_{max}^{abs} = 277 nm (5933 M^{-1} cm^{-1}) and 320 nm (5320 M^{-1} cm^{-1}) for **OEuC-1** and λ_{max}^{abs} = 277 nm (8424 M^{-1} cm^{-1}) and 341 nm (6038 M^{-1} cm^{-1}) for **OEuC-2**, respectively. Moreover, the spectrum of **OEuC-2** exhibited a red shift of 21 nm compared to that of **OEuC-1** presumably due to the enhanced quinoidal character of the electron-donating thienyl ring.[21] Both complexes in the solid state and in DCM solution exhibited bright red emission (Fig. S9–S12, ESI†) under UV excitation (Fig. S13–S16, ESI†) with five innate well-resolved transitions from $^5D_0$ to ^7F_J states (J = 0–4) (Fig. 2 and Fig. S15 and S16†). The photophysical data obtained are presented in Table 1. The complexes displayed similar emission spectra, with the induced electric dipole (ED) $^5D_0 \rightarrow {}^7F_2$ transition contributing ≈85% of the total integrated intensity with a high asymmetric ratio (R_{21}) value, consistent with an asymmetric coordination environment.[18] This is further supported by the large values of Ω_2 = 25.64 × 10^{-20} cm^2 and 26.83 × 10^{-20} cm^2 for **OEuC-1** and **OEuC-2**, respectively, generated by the asymmetric structures of the complexes. Furthermore, the prevalence of the $^5D_0 \rightarrow {}^7F_2$ transition advocates that the forced ED and the dynamic coupling mechanism dominate over the magnetic dipoles (MDs).[22] The excited state lifetime (τ_{obs}) of the $^5D_0$ emitting state for the complexes calculated by the fitting of the decay

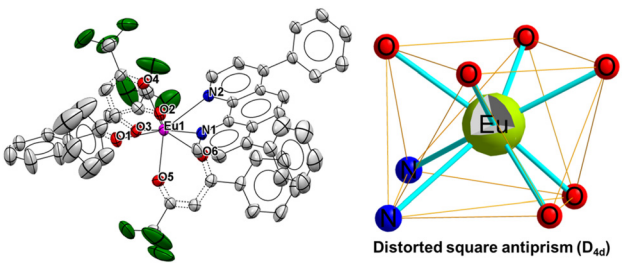

Fig. 1 Single crystal X-ray structure of **OEuC-1** with distorted square antiprism geometry (D_{4d}).

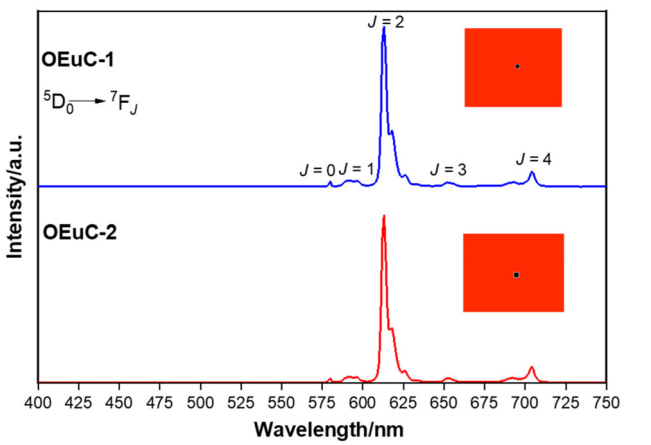

Fig. 2 Solid-state PL emission spectra of the OEuCs. The inset shows a magnified view of the 1931 CIE chromaticity diagram.

Open Access Article. Published on 15 August 2023. Downloaded on 2/10/2026 5:32:21 PM. This article is licensed under a Creative Commons Attribution 3.0 Unported Licence.

Table 1 Photophysical properties of **OEuC-1** and **OEuC-2** in the solid state

Photophysical parameters	OEuC-1	OEuC-2
$^5D_0 \rightarrow {}^7F_0$	17253.97 cm^{-1} [0.74%]	17257.41 cm^{-1} [0.71%]
$^5D_0 \rightarrow {}^7F_1$	16866.49 cm^{-1}	16869.98 cm^{-1}
$^5D_0 \rightarrow {}^7F_2$	16246.87 cm^{-1} [85.51%]	16247.97 cm^{-1} [84.31%]
$^5D_0 \rightarrow {}^7F_3$	15308.77 cm^{-1} [2.78%]	15312.50 cm^{-1} [2.91%]
$^5D_0 \rightarrow {}^7F_4$	14301.46 cm^{-1} [10.96%]	14310.08 cm^{-1} [12.01%]
FWHM of $^5D_0 \rightarrow {}^7F_2$ (nm)	3.76	3.36
Asymmetric ratio (R_{21})[a]	14.71	15.38
$(CIE)_{x,y}$ colour coordinates	0.666; 0.330	0.668, 0.330
τ_{obs}	586.00 ± 2.16 μs (χ^2 = 1.04)	623 ± 0.76 μs (χ^2 = 1.02)
Ω_2 [b] ($\times 10^{-20}$ cm^2)	25.64	26.83
Ω_4 [b] ($\times 10^{-20}$ cm^2)	7.67	8.84
A_{Rad} [c] (s^{-1})	962.04	1018.32
A_{NRad} [c] (s^{-1})	744.44	586.81
τ_R [d] (μs)	1039.50	982
Q^{Eu}_{Eu} [e] (%)	56.38	63.44
Q^{L}_{Eu} (%)	80.00 ± 10	80.09 ± 10
η_{Sen} [f] (%)	70.45	79.21
ΔE ($^3\pi\pi^*$(β-diketone) – $^5D_0$) [cm^{-1}]	4100	3000
ΔE ($^3\pi\pi^*$(Bphen) – $^5D_0$) [cm^{-1}]	3700	3700

Values in the square brackets are % contribution in relation to $^5D_0 \rightarrow {}^7F_1$ MD transition. [a] Ratio of the integrated intensity of the induced electric dipole (ED) $^5D_0 \rightarrow {}^7F_2$ to the $^5D_0 \rightarrow {}^7F_1$ MD transition. [b] Ω_2 and Ω_4 were calculated by applying eqn (1) and (2). [c] A_{Rad} and A_{NRad} were calculated by applying eqn (2)–(4), ESI.† [d] τ_R was calculated by applying eqn (5), ESI.† [e] Q^{Eu}_{Eu} was calculated by applying eqn (6), ESI.† [f] η_{Sen} was calculated by applying eqn (7), ESI.†

curves (Fig. S17–S20, ESI†) lies on the microsecond (μs) timescale (Table 1). Both the OEuCs exhibited high absolute PLQYs in the solid state reaching 80.00 ± 10%, which could be due to the optimum ΔE values (Table 1). To the best of our knowledge, these values are the highest to date for systems with a EuO_6N_2 coordination environment. Interestingly, η_{Sen} of **OEuC-2** is ≈10% higher than that of **OEuC-1**, despite both complexes having similar PLQYs. A plausible explanation is that there is a ≈ 21% reduction in A_{NRad} of **OEuC-2**, which has six fewer C–H oscillators than **OEuC-1**, a factor that is directly related to eqn (7). It may be noted that there are a few nona-coordinated homoleptic Eu(III) complexes[23] bearing anionic tridentate ligands exhibiting PLQY values >80%, reaching up to 94%. However, they possess ultra-long τ_{obs} (1.65 ms–2.74 ms)[23] and thus would have a greater probability of hindering EL performance.

3.3 Electroluminescence and electrophysical properties of OEuC based OLEDs

Good thermal stability of the newly synthesized materials (here **OEuC-1** and **OEuC-2**) is an important pre-requisite for the fabrication of EL devices, since poor thermal stability hampers the device performance along with the operational lifetime at the peak of its operation owing to the Joule heating effect when current flows through the organic layer.[3b,24] The thermal stability of the OEuCs was evaluated in the temperature range of 50 to 700 °C. The thermograms of OEuCs (Fig. S3 & S5, ESI†) revealed that both the OEuCs possess good thermal stability with a T_d (with 5% weight loss) of 315 °C for **OEuC-1** and 330 °C for **OEuC-2**, respectively, implying that they can be readily employed to fabricate EL devices by the vacuum thermal evaporation method. Moreover, the thermal stability of the complexes is well comparable to that of analogous efficient red-emitting complexes *i.e.*, [Eu(btfa)$_3$DPEPO] (T_d = 320 °C),[25] [Eu(nta)$_3$DPEPO] (T_d = 318 °C),[25] and [Eu(btfa)$_3$(Ph-TerPyr] (T_d = 313 °C),[3a] and higher than that of the complexes [Eu(btfa)$_3$]$_2$bpm (T_d = 302 °C),[26] [Eu(tfac)$_3$DPEPO] (T_d = 287 °C °C),[27] [Eu(btfa)$_3$Py-Im] (T_d = 286 °C),[28] [Eu(tfac)$_3$(TB-Im)] (T_d = 241 °C)[3b] and [Eu(hfac)$_3$(TB-Im)] (T_d = 239 °C)[3b] (DPEPO = bis(2-(diphenylphosphino)phenyl)ether oxide; nta = 4,4,4-trifluoro-1-(2-naphthyl)-1,3-butanedione; Ph-TerPyr = 4′-phenyl-2,2′:6′,2″-terpyridine; bpm = 2,2′-bipyrimidine; Py-Im = 2-(2-pyridyl)benzimidazole; tfac = trifluoroacetylacetone; TB-Im = 2-(4-thiazolyl)benzimidazole; hfac = hexafluoroacetylacetone). Encouraged by the excellent photophysical properties and good thermal stability of **OEuC-1** and **OEuC-2** and to demonstrate their potential application as the emitting material in red OLEDs, we have fabricated two single-EML devices (**Devices A** and **E**) with a hole-transporting host CzSi and a fixed doping concentration of OEuCs (2 wt%). The EL spectra, CIE colour diagrams and current density (J)–brightness (B)–voltage (V) curves are shown in the ESI (Fig. S21–S35, ESI†), while the device performance is summarized in Table 2. Both the single-EML devices displayed typical Eu(III) emissions due to the long-range Förster energy transfer (ET) from the host to the complexes and carrier trapping by the OEuCs as observed by one of us.[29] This gains support from the partial overlap of the CzSi emission with the OEuC absorption spectra and the PLQY of **OEuC-1** (2 wt%):CzSi (PLQY = 40%, Table S9, ESI†). Importantly, both devices start illuminating at the same low $V_{turn\text{-}on}$ = 4.4 V implying that the carrier injection and transport abilities of both OEuCs are similar. **Device A** displayed pure red EL with B = 156 cd m^{-2}, CE_{max} = 1.94 cd A^{-1}, PE_{max} = 1.39 lm W^{-1} and $EQE_{max.}$ = 1.10%. Moreover, the EL performance of **Device E** is similar; however, the emitted colour is magenta due to the presence of the CzSi emission. A plausible explanation could be because of the greater electron donating capability of thiophene which may have generated extra electron(s) during the electrical excitation resulting in an imbalance between the electron–hole pair.[30]

To further improve the OLED performance, two double-EML devices (**Devices B** and **F**) with CzSi and another hole-transport and hole-injection TcTa material were fabricated. As expected, the double-EML device of **OEuC-1** (**Device B**) exhibited almost 70% improvement in the CE and EQE with a marginal increase in B = 163 cd m^{-2} compared to **Device A**. The **OEuC-2** based device (**Device F**) also exhibited a three-fold enhancement in the overall performance; however, its colour remained in the light magenta region due to the marginal decrease in host emission *i.e.*, improved ET. To further tune

 This journal is © The Royal Society of Chemistry 2023

Open Access Article. Published on 15 August 2023. Downloaded on 2/10/2026 5:32:21 PM.
This article is licensed under a Creative Commons Attribution 3.0 Unported Licence.

Table 2 Key EL performance of **Devices A–H** of OEuCs

Device	$V_{turn\text{-}on}$ [a]	B_{max} [b]	EQE_{max} [c] (%)	CE_{max} [d]	PE_{max} [e]	FWHM[f]	$(CIE)_{x,y}$	EQE (%)@100 cd m^{-2}
	OEuC-1-based devices							
Device A	4.4	156	1.10	1.94	1.39	6.52	0.608, 0.327	0.09
Device B	3.8	163	1.57	2.78	2.30	6.65	0.611, 0.323	0.11
Device C	3.3	425	4.83	7.89	7.51	6.34	0.630, 0.328	0.67
Device D	3.5	557	5.91	8.58	7.70	6.31	0.636, 0.326	1.18
	OEuC-2-based devices							
Device E	4.4	228	1.08	1.38	0.99	6.00	0.500, 0.300	0.14
Device F	3.5	179	3.63	5.27	4.73	5.97	0.520, 0.300	0.18
Device G	3.2	433	5.01	8.22	8.07	6.00	0.603, 0.320	0.69
Device H	3.4	545	6.24	9.91	9.15	6.02	0.620, 0.323	1.31

[a] Turn-on voltage in volt. [b] Maximum brightness in cd m^{-2}. [c] External quantum efficiency in %. [d] Maximum current efficiency in cd A^{-1}. [e] Maximum power efficiency in lm W^{-1}. [f] Full width at half maxima for $^5D_0 \rightarrow {}^7F_2$ transition in nm under electrical excitation; Commission Internationale de l'éclairage at J = 10 mA cm^{-2}.

the OLED performances, two single-EML and two double-EML OLEDs [**Devices C** and **D** (**OEuC-1**) and **Devices G** and **H** (**OEuC-2**), Fig. S36–S46, ESI†] were fabricated by replacing the unipolar host CzSi with a bipolar host 26DCzPPy (Fig. 3). As can be seen from Table 2, all the devices exhibited red EL (Fig. 4) with low $V_{turn\text{-}on}$ = 3.2–3.5 V. The EL performance of the **OEuC-1** based devices *i.e.*, **Devices C** ($EQE_{max.}$ = 4.83%) and **D** ($EQE_{max.}$ = 5.91%) is more than three times higher than that of **Devices A** ($EQE_{max.}$ = 1.10%) and **B** ($EQE_{max.}$ = 1.57%). Moreover, the **OEuC-2** based **Devices G** and **H** also displayed a similar improvement, which is approximately two times higher than that of the CzSi-based devices (**Devices E** and **F**). It is important to remember that the emission of 26DCzPPy partially overlaps with the absorption spectra of OEuCs (Fig. S47, ESI†), which implies that the carrier trapping process could be the dominant EL process in these devices. To confirm this, we have determined the photophysical properties of the OEuCs : host films (Tables S9 and S10†), which revealed that carrier trapping is the dominant process in the cases of **Devices C**, **D** and **H**, while for **Device G**, both Förster ET and carrier trapping play a crucial role (PLQY = 52.8%). It was also apparent that regardless of the large or small PLQYs of complex : host films (Tables S9 and S10, ESI†), their brightness remains dependent on the excited state lifetime, *e.g.*, **Device A** (PLQY = 40.4%, τ_{obs} = 564.27 μs) and **Device B** (PLQY = 10.3%, τ_{obs} = 566.79 μs) showed similar brightness (Table 2). Importantly, the overall OLED performance of **Device H** is the best among the O_6N_2/O_6O_2 coordinated OEuCs (Chart S3 and Table S11†) with CE_{max} = 9.91 cd A^{-1}, PE_{max} = 9.15 lm W^{-1}, $EQE_{max.}$ = 6.24%, B of 545 cd m^{-2}, and $(CIE)_{x,y}$ = 0.620, 0.323 at J = 10 mA cm^{-2}. Despite the impressive OLED performance of **OEuC-2**-based **Device H** among OEuC-based devices, its EL performance falls behind that of the red-emitting Ir(III) complexes, which usually exhibit EQE >10% at a luminance of 1000 cd m^{-2}.[31] This could be due to the very short excited state lifetime of 0.1–5 μs of Ir(III) complexes[31b] compared to that of the OEuCs (100–800 μs).

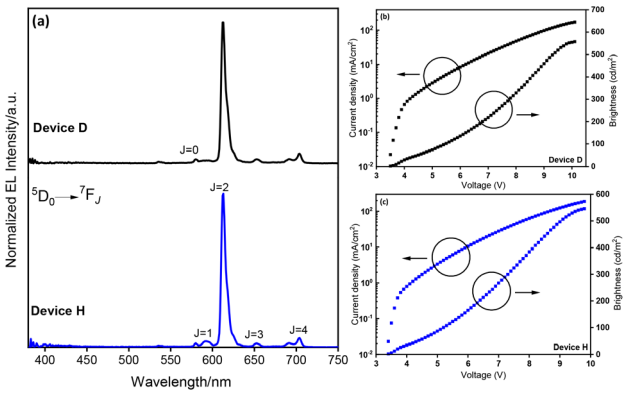

Fig. 4 (a) Normalized EL spectra of **Devices D** and **H** (J = 10 mA cm^{-2}). J–V–B curves of **Devices** (b) **D** and (c) **H**.

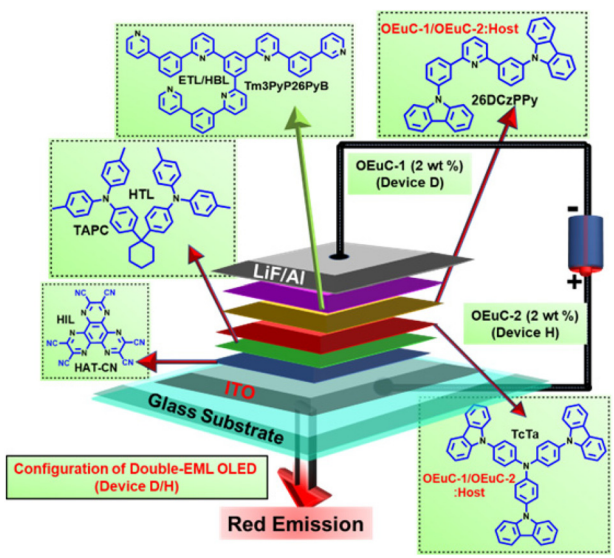

Fig. 3 General device configuration of double-EML OLEDs (HIL: Hole Injection Layer; HTL: Hole Transport Layer; ETL: Electron Transport Layer; HBL: Hole Blocking Layer; HAT-CN: 1,4,5,8,9,11-hexaazatriphenylene hexacarbonitrile; TAPC: di-[4-(*N*,*N*-ditolyl-amino)-phenyl]cyclohexane; Tm3PyP26PyB: 1,3,5-tris(6-(3-(pyridin-3-yl)phenyl)pyridin-2-yl) benzene; host: 26DCzPPy: 2,6-bis(3-(9*H*-carbazol-9-yl)phenyl)pyridine; TcTa: 4,4′,4″-tris(carbazole-9-yl)triphenylamine).

Open Access Article. Published on 15 August 2023. Downloaded on 2/10/2026 5:32:21 PM. This article is licensed under a Creative Commons Attribution 3.0 Unported Licence.

4 Conclusions

We have synthesized two highly luminescent red-emitting OEuCs displaying PLQY = 80% ± 10 and successfully applied them as EMLs to fabricate four single-EML and four double-EML devices. Through the combination of appropriate host materials, the device based on **OEuC-2** (**Device H**) exhibited a remarkable EL performance with CE_{max} = 9.91 cd A^{-1}, PE_{max} = 9.15 lm W^{-1}, $EQE_{max.}$ = 6.24%, B of 545 cd m^{-2}, and $(CIE)_{x,y}$ = 0.620, 0.323 at J = 10 mA cm^{-2}, which, we believe, is the best among the O_6N_2/O_6O_2 coordinated OEuCs (Chart S3 and Table S11†). There are few important observations that we made from the present study: the brightness of the device is independent of the PLQY of the complex : host film but depends on the excited state lifetime of the complex : host film *e.g.*, **Device A** (B = 156 cd m^{-2}, PLQY = 40.4% and τ_{obs} = 564.27 μs) and **Device B** (B = 163 cd m^{-2}, PLQY = 10.3% and τ_{obs} = 566.79 μs) and hole-injection TcTa in conjunction with the bipolar 26DCzPPy material could be an excellent choice of host for OEuCs to develop more efficient R-OLEDs.

Conflicts of interest

There are no conflicts to declare.

Acknowledgements

MSK acknowledges His Majesty's Trust Fund for Strategic Research (Grant No. SR/SQU/SCI/CHEM/21/01) and The Ministry of Higher Education, Research and Innovation (MoHERI), Oman (Grant: RC/RG-SCI/CHEM/22/01) for funding. RI thanks HM's Trust Fund for a postdoctoral fellowship. LZ is grateful for the financial aid from the National Natural Science Foundation of China (62174160). WYW thanks the Hong Kong Research Grants Council (PolyU 15305320), the Guangdong-Hong Kong-Macao Joint Laboratory of Optoelectronic and Magnetic Functional Materials (2019B121205002), the CAS-Croucher Funding Scheme for Joint Laboratories (ZH4A), Hong Kong Polytechnic University, Research Institute for Smart Energy (CDAQ) and the Endowed Professorship in Energy from Miss Clarea Au (847S) for the financial support. PRR is grateful to the Engineering and Physical Sciences Research Council (EPSRC) for funding (Grant EP/K004956/1).

References

1 C. D. S. Brites, A. Millán and L. D. Carlos, in *Handbook on the Physics and Chemistry of Rare Earths*, ed. B. Jean-Claude and K. P. Vitalij, Elsevier, 2016, vol. 49, pp. 339–427.
2 X. Li, J. Gu, Z. Zhou, L. Ma, Y. Tang, J. Gao and Q. Wang, *Chem. Eng. J.*, 2019, **358**, 67–73.
3 (*a*) R. Ilmi, J. Wang, J. D. L. Dutra, L. Zhou, W.-Y. Wong, P. R. Raithby and M. S. Khan, *Chem. – Eur. J.*, 2023, e202300376; (*b*) R. Ilmi, J. Yin, J. D. L. Dutra, N. K. Al Rasbi, W. F. Oliveira, L. Zhou, W. Y. Wong, P. R. Raithby and M. S. Khan, *Dalton Trans.*, 2022, **51**, 14228–14242.
4 K. Binnemans, *Coord. Chem. Rev.*, 2015, **295**, 1–45.
5 L. Wang, Z. Zhao, C. Wei, H. Wei, Z. Liu, Z. Bian and C. Huang, *Adv. Opt. Mater.*, 2019, 1801256.
6 A. Døssing, *Eur. J. Inorg. Chem.*, 2005, **2005**, 1425–1434.
7 K. Nakamura, Y. Hasegawa, H. Kawai, N. Yasuda, Y. Tsukahara and Y. Wada, *Thin Solid Films*, 2008, **516**, 2376–2381.
8 A. S. Kalyakina, V. V. Utochnikova, M. Zimmer, F. Dietrich, A. M. Kaczmarek, R. Van Deun, A. A. Vashchenko, A. S. Goloveshkin, M. Nieger, M. Gerhards, U. Schepers and S. Brase, *Chem. Commun.*, 2018, **54**, 5221–5224.
9 (*a*) R. Ilmi, N. Hasan, J. Liu, D. Mara, R. Van Deun and K. Iftikhar, *J. Photochem. Photobiol., A*, 2017, **347**, 116–129; (*b*) R. Ilmi, A. Haque and M. S. Khan, *J. Photochem. Photobiol., A*, 2019, **370**, 135–144.
10 K. Binnemans, in *Handbook on the Physics and Chemistry of Rare Earths*, ed. J. C. B. K. A. Gschneidner and V. K. Pecharsky, Elsevier, 2005, vol. 35, pp. 107–272.
11 **https://www.rsc.org/periodic-table/**, retrieved 17 April 2023.
12 A. R. Bin Mohd Yusoff, A. J. Huckaba and M. K. Nazeeruddin, *Top. Curr. Chem.*, 2017, **375**, 39.
13 M. S. Khan, R. Ilmi, W. Sun, J. D. L. Dutra, W. F. Oliveira, L. Zhou, W.-Y. Wong and P. R. Raithby, *J. Mater. Chem. C*, 2020, **8**, 5600–5612.
14 (*a*) F. J. Steemers, W. Verboom, D. N. Reinhoudt, E. B. van der Tol and J. W. Verhoeven, *J. Am. Chem. Soc.*, 1995, **117**, 9408–9414; (*b*) M. Latva, H. Takalo, V. M. Mukkala, C. Matachescu, J. C. RodriguezUbis and J. Kankare, *J. Lumin.*, 1997, **75**, 149–169.
15 S. Susumu and W. Masanobu, *Bull. Chem. Soc. Jpn.*, 1970, **43**, 1955–1962.
16 D. B. A. Raj, S. Biju and M. L. P. Reddy, *Inorg. Chem.*, 2008, **47**, 8091–8100.
17 S. Naka, H. Okada, H. Onnagawa and T. Tsutsui, *Appl. Phys. Lett.*, 2000, **76**, 197–199.
18 R. Ilmi, M. S. Khan, Z. Li, L. Zhou, W.-Y. Wong, F. Marken and P. R. Raithby, *Inorg. Chem.*, 2019, **58**, 8316–8331.
19 C. R. Groom, I. J. Bruno, M. P. Lightfoot and S. C. Ward, *Acta Crystallogr., Sect. B: Struct. Sci.*, 2016, **72**, 171–179.
20 (*a*) M. Pinsky, C. Dryzun, D. Casanova, P. Alemany and D. Avnir, *J. Comput. Chem.*, 2008, **29**, 2712–2721; (*b*) D. Casanova, M. Llunell, P. Alemany and S. Alvarez, *Chem. – Eur. J.*, 2005, **11**, 1479–1494.
21 R. Ilmi, H. Al-Sharji and M. S. Khan, *Top. Curr. Chem.*, 2022, **380**, 18.
22 R. Ilmi, S. Anjum, A. Haque and M. S. Khan, *J. Photochem. Photobiol., A*, 2019, **383**, 111968.
23 (*a*) C. Wei, B. Sun, Z. Cai, Z. Zhao, Y. Tan, W. Yan, H. Wei, Z. Liu, Z. Bian and C. Huang, *Inorg. Chem.*, 2018, **57**, 7512–7515; (*b*) Z. Cai, C. Wei, B. Sun, H. Wei, Z. Liu, Z. Bian and C. Huang, *Inorg. Chem. Front.*, 2021, **8**, 41–47.

 This journal is © The Royal Society of Chemistry 2023

Open Access Article. Published on 15 August 2023. Downloaded on 2/10/2026 5:32:21 PM.
This article is licensed under a Creative Commons Attribution 3.0 Unported Licence.

24 R. Ilmi, D. Zhang, L. Tensi, H. Al-Sharji, N. K. Al Rasbi, A. Macchioni, L. Zhou, W.-Y. Wong, P. R. Raithby and M. S. Khan, *Dyes Pigm.*, 2022, **203**, 110300.
25 T. Koizuka, M. Yamamoto, Y. Kitagawa, T. Nakanishi, K. Fushimi and Y. Hasegawa, *Bull. Chem. Soc. Jpn.*, 2017, **90**, 1287–1292.
26 R. Ilmi, W. Sun, J. D. L. Dutra, N. K. Al-Rasbi, L. Zhou, P.-C. Qian, W.-Y. Wong, P. R. Raithby and M. S. Khan, *J. Mater. Chem. C*, 2020, **8**, 9816–9827.
27 R. Ilmi, M. S. Khan, W. Sun, L. Zhou, W.-Y. Wong and P. R. Raithby, *J. Mater. Chem. C*, 2019, **7**, 13966–13975.
28 R. Ilmi, D. Zhang, J. D. L. Dutra, N. Dege, L. Zhou, W.-Y. Wong, P. R. Raithby and M. S. Khan, *Org. Electron.*, 2021, **96**, 106216.
29 L. Zhou, H. Zhang, R. Deng, Z. Li, J. Yu and Z. Guo, *J. Appl. Phys.*, 2007, **102**, 064504.
30 L. Zhou, H. Zhang, W. Shi, R. Deng, Z. Li, J. Yu and Z. Guo, *J. Appl. Phys.*, 2008, **104**, 114507.
31 (*a*) G. Lu, J. Yao, Z. Chen, D. Ma and C. Yang, *J. Mater. Chem. C*, 2020, **8**, 1391–1397; (*b*) T.-Y. Li, J. Wu, Z.-G. Wu, Y.-X. Zheng, J.-L. Zuo and Y. Pan, *Coord. Chem. Rev.*, 2018, **374**, 55–92.